Silicon photonics fiber-to-the-home transceiver array based on transfer-printing-based integration of III-V photodetectors

JING ZHANG,[1,2,*] ANDREAS DE GROOTE,[1,2] AMIN ABBASI,[1,2] RUGGERO LOI,[3] JAMES O'CALLAGHAN,[3] BRIAN CORBETT,[3] ANTÓNIO JOSÉ TRINDADE,[4] CHRISTOPHER A. BOWER,[4] AND GUNTHER ROELKENS[1,2]

[1]Photonics Research Group, Ghent University – imec, Technologiepark 15, 9052 Gent, Belgium
[2]Center for Nano- and Biophotonics, Ghent University, Belgium
[3]Tyndall National Institute, University College Cork, Lee Maltings, Cork, Ireland
[4]X-Celeprint Limited, Cork, Ireland
[*]jingzhan.Zhang@ugent.be

Abstract: A 4-channel silicon photonics transceiver array for Point-to-Point (P2P) fiber-to-the-home (FTTH) optical networks at the central office (CO) side is demonstrated. A III-V O-band photodetector array was integrated onto the silicon photonic transmitter through transfer printing technology, showing a polarization-independent responsivity of 0.39 - 0.49 A/W in the O-band. The integrated PDs (30×40 μm^2 mesa) have a 3 dB bandwidth of 11.5 GHz at -3 V bias. Together with high-speed C-band silicon ring modulators whose bandwidth is up to 15 GHz, operation of the transceiver array at 10 Gbit/s is demonstrated. The use of transfer printing for the integration of the III-V photodetectors allows for an efficient use of III-V material and enables the scalable integration of III-V devices on silicon photonics wafers, thereby reducing their cost.

References and links

1. A. Hatt, O. Zetteberg, K. Ahl, D. Bosshart, R. Montagne, and V. Chillou, "Creating a Brighter Future," in *Proceedings of. FTTH Council Europe Press Conference,* (2014).
2. H. Yamazaki, T. Yamada, K. Suzuki, T. Goh, A. Kaneko, A. Sano, E. Yamada, and Y. Miyamoto, "Integrated 100Gbps PDM-QPSK modulator using a hybrid assembly technique with silica-based PLCs and LiNbO$_3$ phase modulators," in *European Conference on Optical Communication* (ECOC, 2008), paper Mo.3.C.1.
3. R. Nagarajan, D. Lambert, M. Kato, V. Lal, G. Goldfarb, J. Rahn, M. Kuntz, J. Pleumeekers, A. Dentai, H. Tsai, R. Malendevich, M. Missey, K. T. Wu, H. Sun, J. McNicol, J. Tang, J. Zhang, T. Butrie, A. Nilsson, M. Reffle, F. Kish, and D. Welch, "10 channels, 100Gbit/s per channel, dual polarization conherent QPSK monolithic InP receiver photonic integrated circuit," in *Optical Fiber Communication Conference* (OFC, 2011).
4. P. Dong, X. Liu, S. Chandrasekhar, L. Buhl, R. Aroca, and Y. K. Chen, "Monolithic silicon photonic integrated circuits for compact 100+Gb/s coherent optical receivers and transmitters," IEEE J. Sel. Top. Quantum Electron. **20**(4), 6100108 (2014).
5. http://www.europractice-ic.com/SiPhotonics_technology_imec_ISIPP50G.php
6. T. Komljenovic, S. Srinivasan, E. Norberg, M. Davenport, G. Fish, and J. E. Bowers, "Widely tunable narrow-linewidth monolithically integrated external-cavity semiconductor lasers," IEEE J. Sel. Top. Quantum Electron. **21**(6), 1501909 (2015).
7. Y. Jhang, K. Tanabe, S. Iwamoto, and Y. Arakawa, "InAs/GaAs quantum dot lasers on silicon-on-insulator substrated by metal-stripe wafer bonding," IEEE Photonics Technol. Lett. **27**(8), 875–878 (2015).
8. S. Keyvaninia, M. Muneeb, S. Stankovic, R. van Veldhoven, D. van Thourhout, and G. Roelkens, "Ultra-thin DVS-BCB adhesive bonding of III-V wafers, dies and multiple dies to a patterned silicon-on-insulator substrate," Opt. Mater. Express **3**(1), 35–46 (2013).
9. E. Menard, K. Lee, Y. Khang, R. Nuzzo, and J. Rogers, "A printable form of silicon for high performance thin film transistors on plastic substrates," Appl. Phys. Lett. **84**(26), 5398–5400 (2004).
10. A. De Groote, P. Cardile, A. Z. Subramanian, A. M. Fecioru, C. Bower, D. Delbeke, R. Baets, and G. Roelkens, "Transfer-printing-based integration of single-mode waveguide-coupled III-V-on-silicon broadband light emitters," Opt. Express **24**(13), 13754–13762 (2016).

11. R. Loi, J. O'Callaghan, B. Roycroft, C. Robert, A. Fecioru, A. J. Trindade, A. Gocalinska, E. Pelucchi, C. A. Bower, and B. Corbett, "Transfer Printing of AlGaInAs/InP Etched Facet Lasers to Si Substrates," IEEE Photonics J. **8**(6), 1504810 (2016).
12. J. Justice, C. Bower, M. Meitl, M. Mooney, M. Gubbins, and B. Corbett, "Wafer-scale integration of group III-V lasers on silicon using transfer printing of epitaxial layers," Nat. Photonics **6**(9), 610–614 (2012).
13. H. Yang, D. Zhao, S. Chuwongin, J.-H. Seo, W. Yang, Y. Shuai, J. Berggren, M. Hammar, Z. Ma, and W. Zhou, "Transfer-printed stacked nanomembrane lasers on silicon," Nat. Photonics **6**(9), 615–620 (2012).
14. D. Vermeulen, T. Spuesens, P. De Heyn, P. Mechet, R. Nötzel, S. Verstuyft, D. Van Thourhout, and G. Roelkens, "III-V/silicon-on-insulator photonic integrated circuit for fiber-to-the-home central office transceivers in a point-to-point network configuration," in *36th European Conference and Exhibition on Optical Communication* (ECOC, 2010).
15. T. Kusserow, S. Ferwana, T. Nakamura, T. Hayakawa, N. Dharmarasu, B. Vengatesan, and H. Hillmer, "Micromachining of InP/InGaAs multiple membrane/airgap structures for tunable optical devices," Proc. SPIE **6993**, 69930B (2008).
16. D. Vermeulen, S. Selvaraja, P. Verheyen, G. Lepage, W. Bogaerts, P. Absil, D. Van Thourhout, and G. Roelkens, "High-efficiency fiber-to-chip grating couplers realized using an advanced CMOS-compatible silicon-on-insulator platform," Opt. Express **18**(17), 18278–18283 (2010).
17. H. Chen, *Advanced Germanium p-i-n Avalanche Photodetectors for Low-power Optical Interconnects* (2016), Chap. 1.

1. Introduction

Ethernet point-to-point (P2P) access networks, with advantages such as a simple architecture, no need of expensive wavelength division multiplexing (WDM) components and the ease to upgrade, are mostly deployed in Europe [1]. In such access networks, each optical network unit located in the home of the subscriber is directly connected to a dedicated transceiver in the central office (CO), therefore requiring a large number of CO transceivers. In order to keep size and power consumption of such a CO manageable, the realization of integrated, low cost and low power consumption transceiver arrays is of paramount importance. Among several mainstream photonic integration platforms including silica-on-silicon (SOS) [2], InP [3] and silicon-on-insulator (SOI) [4], SOI has the obvious advantages of CMOS compatibility and high refractive index contrast, which allows high-volume production of compact photonic circuits with strong light-matter interaction, resulting in low cost, low power consumption and high bandwidth devices. The imec silicon photonics platform [5], amongst other platforms, enables the integration of high-speed devices such as Ge photodetectors (PDs), ring modulators, Mach-Zehnder modulators. Together with mature passive building blocks such a platform is well-suited for the integration of high-speed optical transceivers and transceiver arrays. For the CO transceiver array an O-band receiver is required. Although Ge PDs are a good candidate for this function, the issue of realizing a polarization-independent data signal reception and the duplexing with the C band downstream signal results in a complex integrated circuit. Instead of Germanium, III-V semiconductor material can be used for the same purpose. As shown in Fig. 1, by integrating a surface illuminated O-band photodetector on top of the fiber-to-chip grating coupler, the O-band upstream signal can be received in a polarization independent way. By choosing the cut-off wavelength of the photodetector between the O-band and C-band, the C-band downstream signal can be coupled to fiber through the photodetector structure, without being absorbed, providing a straightforward path to optical duplexing. In order to cost-effectively integrate the III-V photodetectors on the silicon photonic wafers, wafer-scale processes are required. In conventional bonding technologies relying on die-to-wafer and wafer-to-wafer bonding [6–8] the efficiency of III-V material use is poor as only a very small fraction of the eventual chip surface requires III-V device structures. Transfer printing, as a novel technique, was first proposed in 2004 [9]. By utilizing this technique, micron-scale thin films such as III-V material coupons and devices [10–13] can be transferred from a source substrate to a target substrate with high alignment accuracy (+/−1.5 μm 3σ). More information on the transfer printing process of III-V coupons can be found in [10]. Since the material coupons/devices can be wafer-scale pre-defined in a dense array on the III-V source wafer and picked-up and printed in a massively parallel way, the efficiency of the usage of source material is

significantly improved and the cost of the integration is greatly reduced. In the case of transfer printing of pre-processed opto-electronic components, the integration post-processing just consists of a passivation and collective wiring of the devices. Moreover, the technique paves the way to integrate devices from different source wafers.

In this paper we present the realization of a 4-channel silicon photonic transceiver array for P2P FTTH optical networks, operating at 10 Gbit/s per channel. An array of III-V O-band photodetectors (PDs) was integrated with the silicon photonics circuit. We previously demonstrated the use of such PDs for a single channel transceiver where the integration was realized through bonding technology [14]. In this work, the PDs were integrated on top of the grating couplers of 4 channels through the transfer printing approach. This work showcases the great potential that transfer printing has for the integration of III-V opto-electronic components on a silicon photonic integrated circuit wafer.

2. Transceiver configuration

The schematic layout the proposed 4-channel transceiver array is depicted in Fig. 1(a). The silicon photonic integrated circuit is realized in imec's iSIPP25G platform. A 1550 nm CW laser is coupled to the silicon photonic transceiver, where it is split to 4 channels through cascaded 1×2 MMIs. Each of the channels has a silicon ring modulator, which serves as a downstream transmitter, to imprint the downstream data on the carrier (1550 nm). The signal is then coupled to fiber through the grating coupler and the integrated O-band PD, as shown in Fig. 1(b). By selecting the cut-off wavelength of the III-V absorbing material to be 1.37 μm, the PDs are 'transparent' (4 orders of magnitude smaller responsivity) for the C-band signal, enabling the duplexing of the C-band and O-band signal that are sent and received through the same fiber. Thanks to the vertical coupling scheme, the PDs have a polarization-independent responsivity of 0.39-0.49 A/W in the O-band.
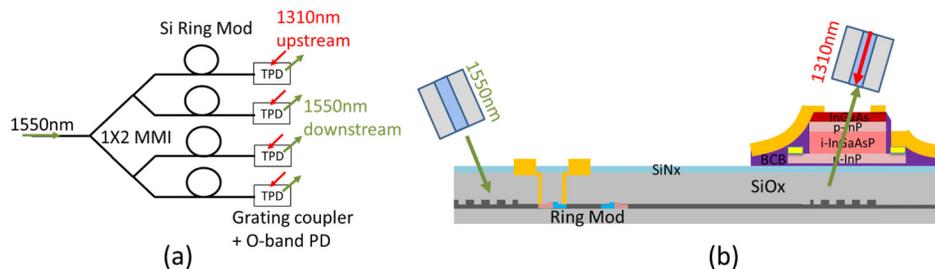
Fig. 1. (a) Schematic layout of the III-V-on-silicon FTTH transceiver array, (b) Schematic cross-section of one transceiver. TPD: transparent photodetector.

3. Transfer printing pre-fabricated PDs on Si PIC

The key process discussed in this work is the transfer printing of the III-V photodetectors on the silicon photonic integrated circuit. As shown in Table 1, the III-V O-band PD layer stack consists of a 1 μm intrinsic InGaAsP absorbing layer with a cut-off wavelength of 1.37 μm. Besides the classical p-i-n layer structure, a 1 μm InGaAs layer is used for releasing the pre-fabricated PDs. Instead of highly doped InP hereby a 60 nm thick intrinsic InP is used as the etch stop layer [11, 15].

The transfer-printing-based integration process flow is described in Fig. 2. Figure 2(a) shows the full layer stack of the source wafer. Firstly the top sacrificial layer was removed by a short etch in HCl. In order to simplify the post-process after transfer printing, a U-shaped Ti/Au contact was defined, leaving a 17 μm wide absorption window for the reception of the upstream and the transmission of the downstream signal from and to the same fiber, respectively. The 30×40 μm² PD mesa is defined using ICP using a 200 nm thick SiNx hard mask. After reaching the n-contact layer, a second mesa was defined by patterning the n-InP

layer and a Ni/Ge/Au contact surrounding the PD mesa is defined. With a second SiNx hard mask the InGaAs release layer was etched through slightly into the InP substrate, as shown in Fig. 2(f). Then the PD structures were encapsulated by a photoresist layer (~2.5 μm thick) with narrow tethers anchored to the substrate (Fig. 2(g)). At this moment, the source wafer is ready for release. An aqueous FeCl$_3$ solution at 5 °C that has a selectively of 1000 for the etching of InGaAs with respect to intrinsic InP was used to undercut the pre-fabricated PDs, resulting in a flat bottom surface after the release etch, which guarantees a good bonding quality when transferred to the SOI waveguide circuit (Fig. 2(h)). A 50 nm DVS-BCB layer was spin coated on the planarized SOI waveguide circuit, followed by a 150 °C soft-bake. Now the PDs on the III-V wafer and the target substrate (SOI) are ready for the transfer printing integration. In this process, a PDMS stamp with a 50×50 μm^2 post was used to pick-up and transfer the PDs using an X-Celeprint μTP-100 tool (Figs. 2(i) and 2(j)).

Table 1. III-V layer stack for the O-band PD.

Layer	Thickness	Material	Doping (cm^3)	Function
10	100nm	InP	n.i.d	cap-layer
9	100nm	InGaAs	$>1 \times 10^{19}$	p-contact
8	200nm	InGaAs	1×10^{19}	p-contact
7	300nm	InP	5×10^{17}	p-cladding
6	1000nm	InGaAsP	n.i.d.	absorption
5	240nm	InP	1×10^{18}	n-contact
4	60nm	InP	n.i.d.	etch stop
3	1000nm	InGaAs	n.i.d.	release
2	150nm	InP	n.i.d	buffer
1		InP	n-type	substrate
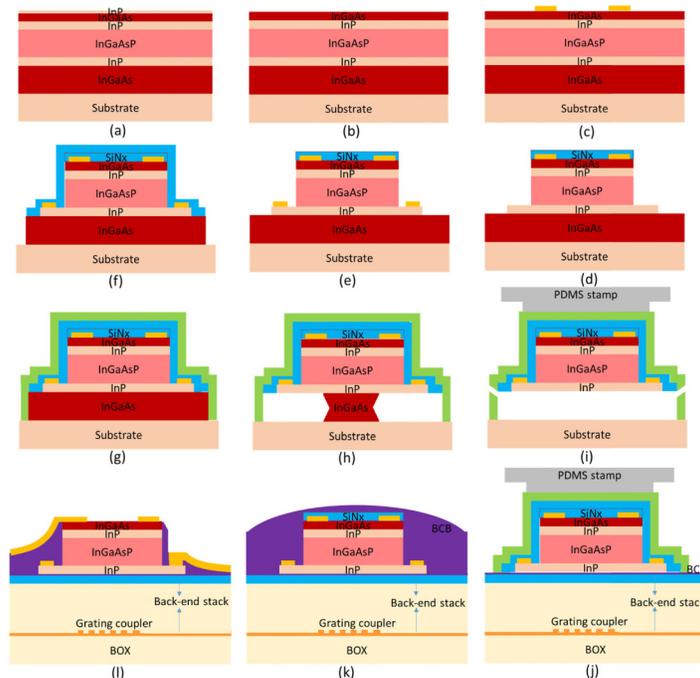
Fig. 2. Process flow of transfer-printing-based integration of O-band III-V PDs on silicon photonic integrated circuits. (a) The initial III-V layer stack, (b) Sacrificial layer removal, (c) P contact metal deposition, (d) Definition of the PD mesa, (e) Definition of the second mesa and n-contact metal deposition, (f) Shaping the release area, (g) Encapsulation and tether definition, (h) Under etching of the release layer, (i) Picking up pre-fabricated PDs from the InP substrate, (j) Auto-alignment to grating coupler and printing, (k) BCB planarization, (l) Final metallization.

The operation principle of transfer printing is based on the visco-elastic behavior of the PDMS stamp. The PDs are picked up from the InP substrate by lifting up the stamp rapidly, thereby breaking the tethers that anchored the device to the III-V source wafer. Printing is done by slowly lifting the stamp and applying a shear force to detach the stamp from the PD. Thanks to the auto-alignment module with pattern recognition function, the PDs were automatically center-to-center aligned and printed on top of the grating couplers with an accuracy of -/+ 1.5 μm. After transfer printing, the photoresist on top of the PDs was removed by oxygen plasma using RIE and the DVS-BCB was cured at 270 °C. To passivate the device, a DVS-BCB layer was spin coated and fully cured again (Fig. 2(k)). After thinning down the BCB layer to the P contact metal and opening vias to reach the N contact metal, the process is completed by a thick Ti/Au deposition to wire the PD contacts to a bond pad array (Fig. 2(l)). Figures 3(a) and 3(b) show the microscope images of the pre-fabricated PD array and a single PD on the InP source wafer after release etch. Different types of tethers, as shows in Fig. 3(a), were demonstrated to be working well. The final realized receiver array is shown in Fig. 3(c).
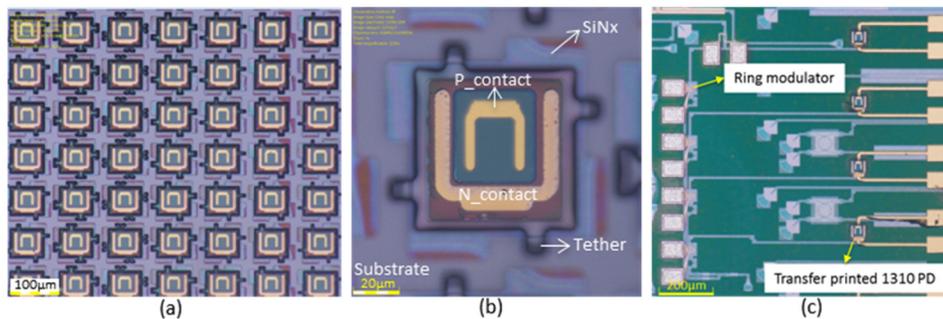
Fig. 3. The PDs before and after transfer printing, (a) Microscopic image of a pre-fabricated PD array on III-V source wafer, (b) A zoom-in image of one PD on the source wafer showing the design of the tether structures, (c) Final realized transceiver with bond pad array.

4. Transceiver characterization

4.1 Static characterization

Figure 4(a) shows the transmission of each channel (cascaded MMIs, microring and O-band PDs, excluding the loss from grating couplers). As the two cascaded 1×2 MMIs introduce ~6.5 dB loss for each channel at 1550 nm, the insertion loss of the O band PDs for the C band signal is around 3.5 dB at 1550nm, that is mainly from the absorption of the p-contact layer (~0.9 dB), the reflections at the interfaces between p-contact layer and air (~1.67 dB) and between the BCB and n-contact layer (0.55 dB). Together with the 4 dB insertion loss from each grating coupler, which can be improved to be less than −2 dB with optimized design [16], the overall insertion loss for each channel is 18 dB. Figure 4(b) shows a DC characterization of the p-i-n ring modulator, revealing a 12.3 dB extinction ratio for a 2.5 Vpp voltage swing.
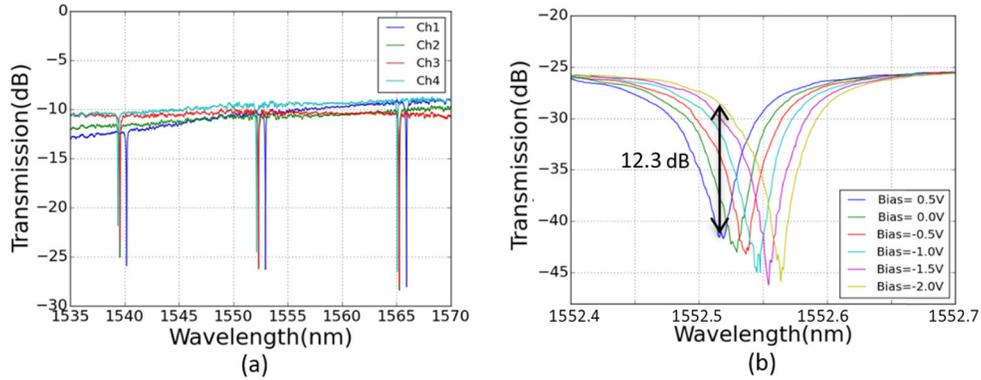
Fig. 4. (a) The loss of the trancevier (microring, cascaded MMIs and O band PD) in C-band excluding the loss from grating couplers, (b) The ring modulator resonate wavelength shift versus bias voltage.
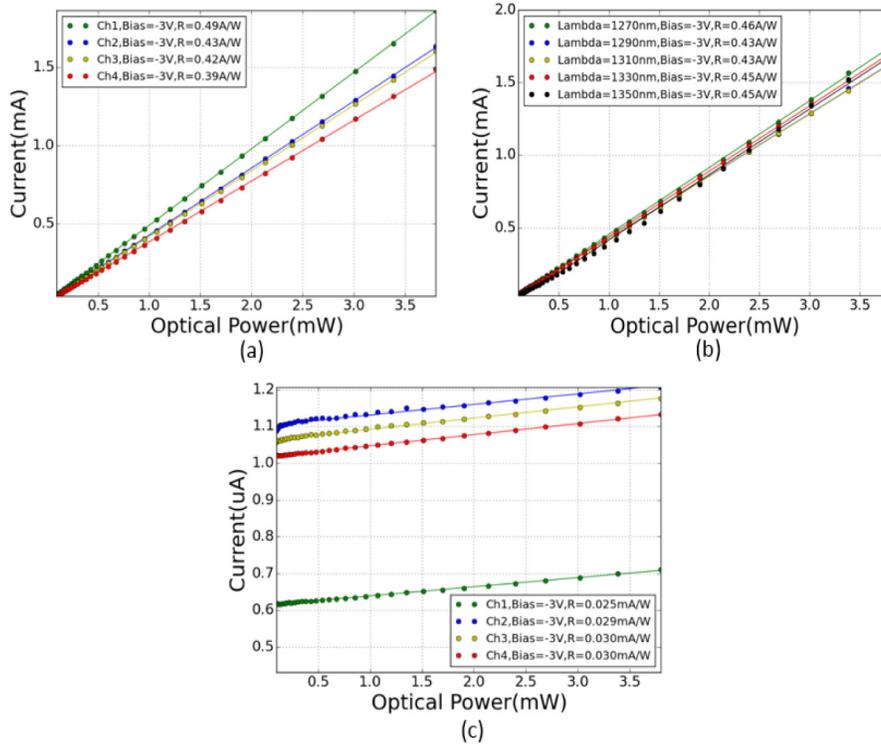
Fig. 5. Photocurrent of the transfer printed O-band PDs (a) at 1310 nm, (b) over the range of 1270 nm-1350 nm, (c) at 1550 nm (including the photodetector dark current).

Of key importance for the operation of the transceiver is the transparency of the photodetector for the downstream C-band signal. This was verified under CW conditions, as shown in Fig. 5. As a bias of −3 V was applied during the dynamic measurements, all the static characterizations were done at the same −3 V bias. The responsivity for the O-band signal is 0.39-0.49 A/W (Fig. 5(a)) and it is quite constant over the range from 1270 nm to 1350 nm wavelength (Fig. 5(b)), while that for the C-band signal is 0.025-0.03 mA/W, which is more than four orders of magnitude smaller (Fig. 5(c)). The dark current of the integrated

O-band PDs varies from 0.6 to 1.1 µA. This however is not expected to impact the system performance when integrated with a transimpedance amplifier array [17].

4.2 Dynamic characterization

In order to verify the high-speed performance of the transceiver array, small signal characterization using a Vector Network Analyzer (VNA) was at first carried out. As a standard building block in the imec's iSIPP25G platform, the ring modulators have a bandwidth of 15 GHz at −1 V bias, as shown in Fig. 6(a). On the other hand for the transfer printed O-band PDs the 3 dB bandwidth is measured to be 11.5 GHz in Fig. 6(b), with good uniformity over the 4 devices.
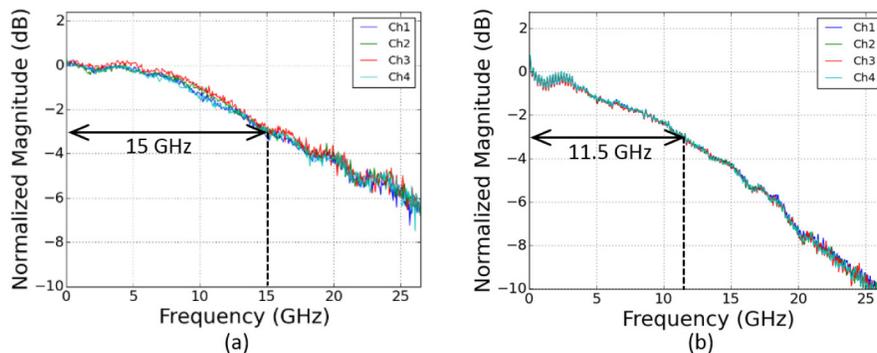
Fig. 6. Small-signal response. (a) Measured $|S21|^2$ curves of ring modulators. (b) Measured $|S21|^2$ curves of O band PDs.
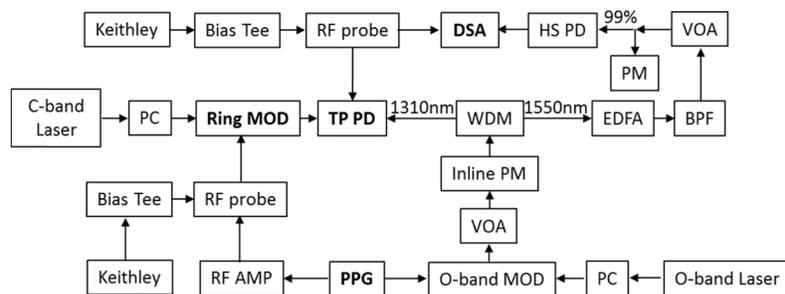
Fig. 7. Schematic layout of the characterization setup for the transceiver operating with upstream and downstream signal simultaneously applied. DSA: digital serial analyzer; HS PD: high-speed photodetector; VOA: variable optical attenuator; PM: power monitor; MOD: modulator; TP PD: transfer printed photodetector; WDM: wavelength division multiplexer; EDFA: erbium doped fiber amplifier; BPF: band pass filter; PPG: pulse pattern generator; PC: polarization controller.

   Figure 7 depicts the schematic layout of the measurement setup. Back-to-back characterization was carried out in this work. A C-band and an O-band tunable laser were employed as the downstream and upstream carrier sources, respectively. The silicon ring modulator and an O-band commercial modulator were simultaneously driven by a pulse pattern generator. A 1310 nm/1550 nm fiber wavelength multiplexer was used for duplexing the O-band and C-band signals. The transmitted C band data signal was detected using a commercial high-speed photodetector after being boosted by an erbium doped fiber amplifier and filtered by a band pass filter to suppress amplified spontaneous emission noise. The bias for the silicon ring modulator and transfer printed O-band photodetector was applied through a bias tee. Variable optical attenuators were used to adjust the power in fiber while an inline power meter and a power meter connected to a −20 dB power tap were inserted in the link to

monitor the actual optical power coupled to the transfer printed photodetector (O-band) and received by the high-speed photodetector (C-band), respectively. Finally, the electric signals were fed to a digital serial analyzer for eye diagram analysis.

During the measurement the transmitter (Ring MOD) and receiver (TP PD) were operating at the same speed. A non-return-to-zero pseudo-random-bit-sequence generated by the pulse pattern generator at 10 Gbit/s was used for the high-speed characterization. The C band laser emits 0 dBm at 1550 nm, resulting in around −15 dBm optical power coupled to each ring modulator. The output power of the O-band laser was set to 13 dBm and the average power on the photodetector is adjusted by the VOA. A −1 V bias and a voltage swing of 1.6 V, which provided the optimized performance, were applied to the Ring MOD. With an average optical power of 0 dBm feeding to the HS PD, the C-band eye diagrams indicate an extinction ratio of 9.2-9.75 dB for these four channels with Q factor of around 10. Figure 8 shows overlaid eye diagrams of the upstream (O-band) and downstream (C-band) signals. By varying the polarization of the upstream signal a small peak-to-peak amplitude variation of 6% could be observed for the O-band PDs. This is attributed to the non-vertical position (13 degrees off-vertical) of the fiber. In order to check the wavelength dependence of the TP PDs, the operation wavelength was swept from 1270 nm to 1350 nm. Figures 9(a)-9(c) show the eye diagrams for 1270 nm, 1310 nm and 1350 nm data signals, respectively. Clean and open eyes were obtained for all the TP PDs over the entire wavelength range. A narrower eye was observed at 1350 nm due to the high loss of the wavelength multiplexer at this wavelength.
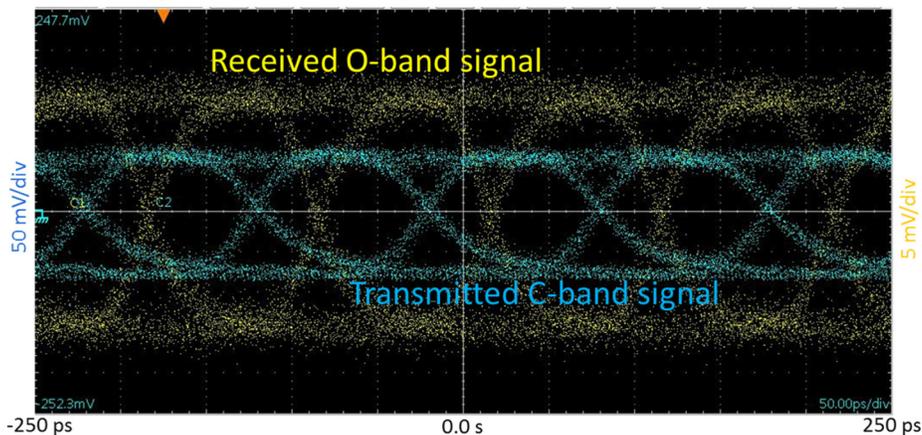
Fig. 8. Overlaid 10 Gbit/s eye diagrams of the upstream (O-band) data signal and downstream (C-band) data signal.
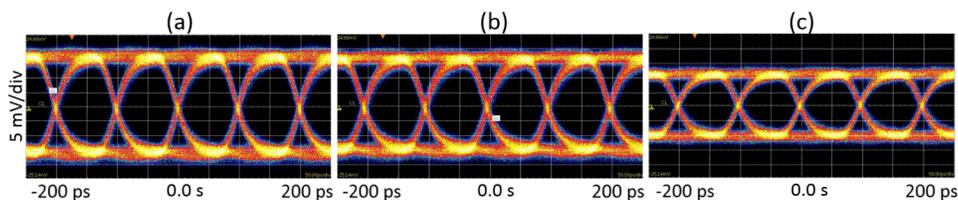
Fig. 9. Received 10 Gbit/s NRZ-PRBS upstream signal at (a) 1270 nm, (b) 1310 nm and (c) 1350 nm. The vertical scale is identical in all plots

As the bandwidth of the ring modulators and the O band PDs is above 10 GHz, up to 20 Gbit/s operation should be possible. Limited by the maximum speed (12.5 Gbit/s) of the pulse pattern generator, the bit error rate was investigated at 10 Gbit/s and 12.5 Gbit/s with different pattern lengths. Firstly, the received power on the O band PDs was adjusted through the VOA, while having the upstream link operational. As shown in Fig. 10, the receivers behaved

uniformly and error free operation was achieved at a received power of 0 dBm for a pattern length of 2^7-1. When a longer pattern length (2^{15}-1) or a higher speed (12.5 Gbit/s) was used, the required input power for error free operation increase to 1 and 2.7 dBm, respectively. The high average power required is due to the lack of integrated transimpedance amplifier. Vice versa, the bit error rate of the downstream link was studied and error-free operation was realized at an input power of −11 dBm for 10 Gbit/s operation (2^7-1). In order the check the C-band/O-band crosstalk in the O-band PD in a straight forward way, a comparison between bit error rate results with the ring modulator on and off was made and no obvious change was observed from the curves shown in Fig. 11.
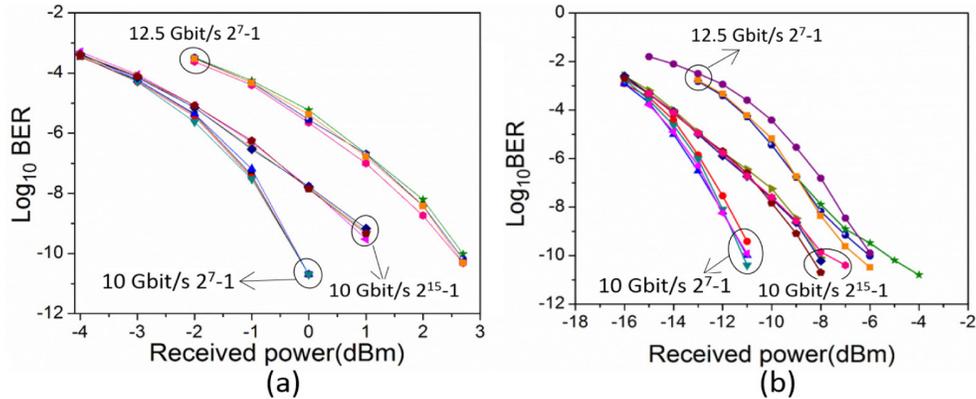
Fig. 10. Measured BER versus received optical power for (a) the upstream data signal, (b) the downstream data signal.
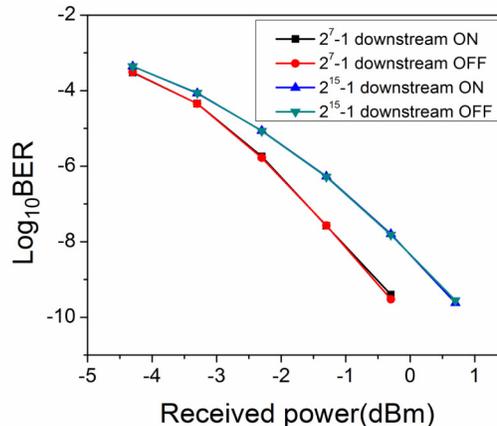
Fig. 11. Measured bit error rate of the upstream data signal at 10 Gbit/s with the downstream link operational or off.

5. Conclusion

In this paper we present a 4 channel transceiver for a point-to-point FTTH network at the central office side. The up-stream (O-band) receivers were realized by the integration of III-V through a transfer printing technique. To our knowledge this is the first time that the transfer-printing-based integration of pre-fabricated devices on integrated photonic circuits is demonstrated. A responsivity of 0.39-0.49 A/W was obtained with four orders of magnitude lower responsivity of the C-band signal, allowing a low cross talk between upstream and downstream data signals. Error-free operation for a 2^7-1 data stream at 10 Gbit/s was realized at a received power of 0 dBm and −11 dBm for upstream (without transimpedance amplifier)

and downstream (with transimpedance amplifier) data signals, respectively. The efficient use of III-V material in the integration and the high accuracy alignment of the transfer printing system, makes the transfer printing technique promising for high yield, low-cost and wafer scale integration of III-V opto-electronic components on silicon photonic integrated circuits.

Funding

Acknowledgments